

# Graphene Multilayer Supported Gold Nanoparticles for Efficient Electrocatalysts Toward Methanol Oxidation

Yuri Choi, Minsu Gu, Jongnam Park, Hyun-Kon Song, and Byeong-Su Kim\*

This study reports a simple method of integrating electroactive gold nanoparticles (Au NPs) with graphene oxide (GO) nanosheet support by layer-by-layer (LbL) assembly for the creation of 3-dimensional electrocatalytic thin films that are active toward methanol oxidation. This approach involves the alternating assembly of two oppositely charged suspensions of Au NPs with GO nanosheets based on electrostatic interactions. The GO nanosheets not only serve as structural components of the multilayer thin film, but also potentially improve the utilization and dispersion of Au NPs by taking advantages of the high catalytic surface area and the electronic conduction of graphene nanosheets. Furthermore, it is found that the electrocatalytic activity of the multilayer thin films of Au NPs with graphene nanosheet is highly tunable with respect to the number of bilayers and thermal treatment, benefiting from the advantageous features of LbL assembly. Because of the highly versatile and tunable properties of LbL assembled thin films coupled with electrocatalytic NPs, we anticipate that the general concept presented here will offer new types of electroactive catalysts for direct methanol fuel cells.

## 1. Introduction

Harnessing energy from green resources and developing suitable storage systems are the top priorities in current researches on energy systems. Direct methanol fuel cells (DMFCs) have received a considerable attention as an attractive power source for various systems due to their high energy density, ease of handling and processing, low operation temperatures and environmental benignity.<sup>[1–3]</sup> Despite significant progress in the development of efficient DMFCs, it is desirable to develop highly efficient and cost-effective electrocatalysts for key reaction in DMFCs such as methanol oxidation.<sup>[4–6]</sup> Although platinum or its alloys are the most popular choices for electrocatalysts, they usually suffer from several disadvantages such as poisoning effect, corrosion to some electrolytes, and high cost, all of which hamper the commercialization of DMFCs.<sup>[7–10]</sup> Therefore, recent efforts have been geared toward the development of more efficient catalyst without compromising the performance of the

devices. Recently, the unique properties of gold nanoparticles (Au NPs) were found to exhibit superior electrocatalytic activity towards CO oxidation, methanol oxidation, water gas shift reaction, and electro-oxidation.<sup>[11–14]</sup> However, there are still obstacles in utilizing Au NPs because they often experience irreversible aggregation during electrocatalytic cycles, leading to a significant loss of nanoscale catalytic effect. Thus, they need a proper electrocatalytic support in order to preserve the intrinsic surface properties as it is known that the support materials have a strong influence on the electrocatalytic activity of the NPs.<sup>[15–17]</sup>

Among many potential candidates for electrocatalytic support, graphene, a monolayer of two-dimensional carbon lattice, is an appealing choice with its remarkable electrical, thermal, and mechanical properties.<sup>[18–20]</sup> In particular, solution processable graphene nanosheets typically prepared by chemical exfoliation present unique advantages in a controlled, scalable, and reproducible production of single sheet graphene dispersions.<sup>[21–23]</sup> Taking full advantage of the surface functional groups and high conductivity together with its high specific surface area, graphene nanosheet is an excellent substrate for hosting and growing nanomaterials for high-performance electrochemical and electrocatalytic applications.<sup>[15,24]</sup> A number of examples have been reported to host a variety of metal, metal oxide, semiconducting, and magnetic nanoparticles on the surface of graphene nanosheets for the creation of electroactive hybrid nanomaterials;<sup>[25–29]</sup> however, few papers have reported the utilization of Au NPs anchored on the graphene nanosheets and its electrocatalytic activity.<sup>[30]</sup>

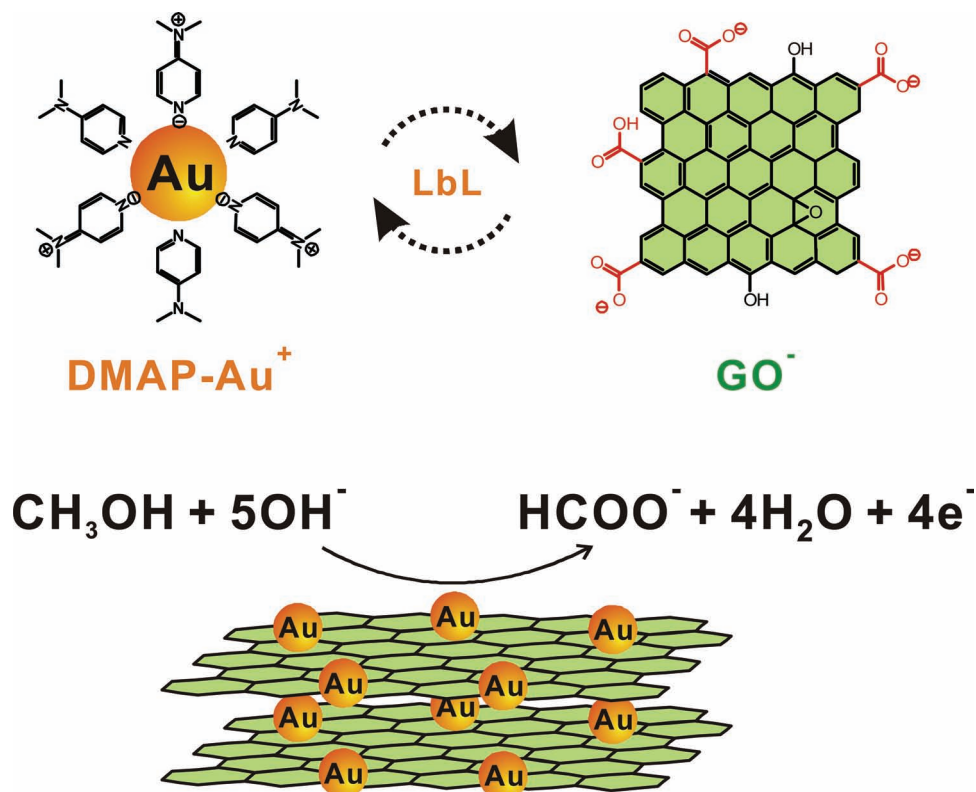
In that regard, layer-by-layer (LbL) assembly offers a variety of opportunities for preparing multilayer thin films of desired functions with a nanometer scale control over the composition and thickness as a true nanoscale blending method.<sup>[31–32]</sup> The integration of graphenes and related nanostructures into multilayer films by LbL assembly has been recently demonstrated from a number of examples;<sup>[33–35]</sup> yet, many of these studies are limited in creating electrically conducting structures and utilizing them in transparent electrodes. Herein, we report the integration of electroactive Au NPs with a graphene oxide nanosheet support by LbL assembly for the creation of 3-dimensional electrocatalytic thin films that are active toward methanol oxidation (Scheme 1).

In specific, positively charged 4-dimethylaminopyridine (DMAP) coated Au NPs and negatively charged graphene oxide (GO) nanosheets are assembled based on the electrostatic

Y. Choi, M. Gu, Prof. J. Park, Prof. H.-K. Song,  
Prof. B.-S. Kim  
Interdisciplinary School of Green Energy  
KIER-UNIST Advanced Center for Energy  
and Low Dimensional Carbon Materials Center  
Ulsan National Institute of Science  
and Technology (UNIST)  
Ulsan 689-798, Korea  
E-mail: bskim19@unist.ac.kr



DOI: 10.1002/aenm.201200214



**Scheme 1.** Schematic representation of layer-by-layer (LbL) assembled  $(\text{Au}/\text{GO})_n$  multilayer thin film for methanol oxidation.

interactions on a silicon wafer or ITO-coated glass to afford the multilayer thin films of Au NPs supported by GO nanosheets. In this study, the GO nanosheet not only serves as a structural component of the multilayer thin film, but also potentially improves the utilization and dispersion of Au NP catalysts by taking advantages of high catalytic surface area, chemical stability, and the electronic conduction of graphene nanosheet. Furthermore, we found that the electrocatalytic activity of the multilayer thin films of Au NPs with graphene nanosheet is highly tunable with respect to the number of bilayers, assembly conditions, and post-treatment, benefiting from the advantageous features of LbL assembly. Here we choose the Au NPs for their mature synthetic protocols and fine catalytic activity, yet this method can be readily extended to other NPs of sufficient surface charges that can be assembled by electrostatic LbL assembly. Considering the wide-ranging potential applications of two-dimensional graphene sheets as host material for a variety of NPs, the approach developed here may lead to new possibilities for the fabrication of hybrid NP-graphene structures endowed with multiple functionalities.

## 2. Results and Discussion

In order to introduce the GO into an LbL system based on the electrostatic interactions, a negatively charged GO suspension was initially prepared according to the modified Hummers method from a commercially available graphite powder.<sup>[36]</sup> Following sonication for exfoliation of the graphite oxide, the

chemical functional groups introduced on the surface of the graphene sheet such as carboxylic acids rendered the prepared GO suspension negatively charged over a wide range of pH conditions and displayed the pH-responsive features. Consistent with other reports, the changes of  $\zeta$ -potential with external pH conditions are typical characteristics for weak polyelectrolytes that allow the tuning of internal structures within the multilayer thin film.<sup>[37]</sup> Atomic force microscopy (AFM) further revealed that the prepared GO suspension mainly comprised a single-layer graphene nanosheet having a thickness of approximately 0.70 nm with lateral dimensions of 0.70–1.5  $\mu\text{m}$  (Figure S1). Subsequently, positively charged Au NPs were prepared based on the spontaneous phase transfer of organic soluble Au NPs across the aqueous phase using 4-dimethylaminopyridine (DMAP), a readily available organic ligand that affords the necessary stability in aqueous solution.<sup>[38]</sup> The resulting DMAP-coated Au NPs had an average diameter of 6 nm with a high surface potential of +35 mV at pH 11.

With these two stable suspensions of Au NPs and GO, we have fabricated multilayer films by repeatedly dip-coating onto a planar silicon substrate or ITO-coated glass slide to afford the multilayer in an architecture of  $(\text{Au}/\text{GO})_n$  ( $n$  = number of bilayers (BL), typically  $n = 2 - 10$ ) (Figure 1). After the LbL assembly, the multilayer thin films of  $(\text{Au}/\text{GO})_n$  were subjected to a mild thermal reduction process to restore the electrical conductivity according to the previous protocols.<sup>[39–40]</sup> Moreover, we postulate here that the DMAP ligands that were present on the surface of Au NPs would prevent the effective electrocatalytic activity during the oxidation of methanol, as it is well known

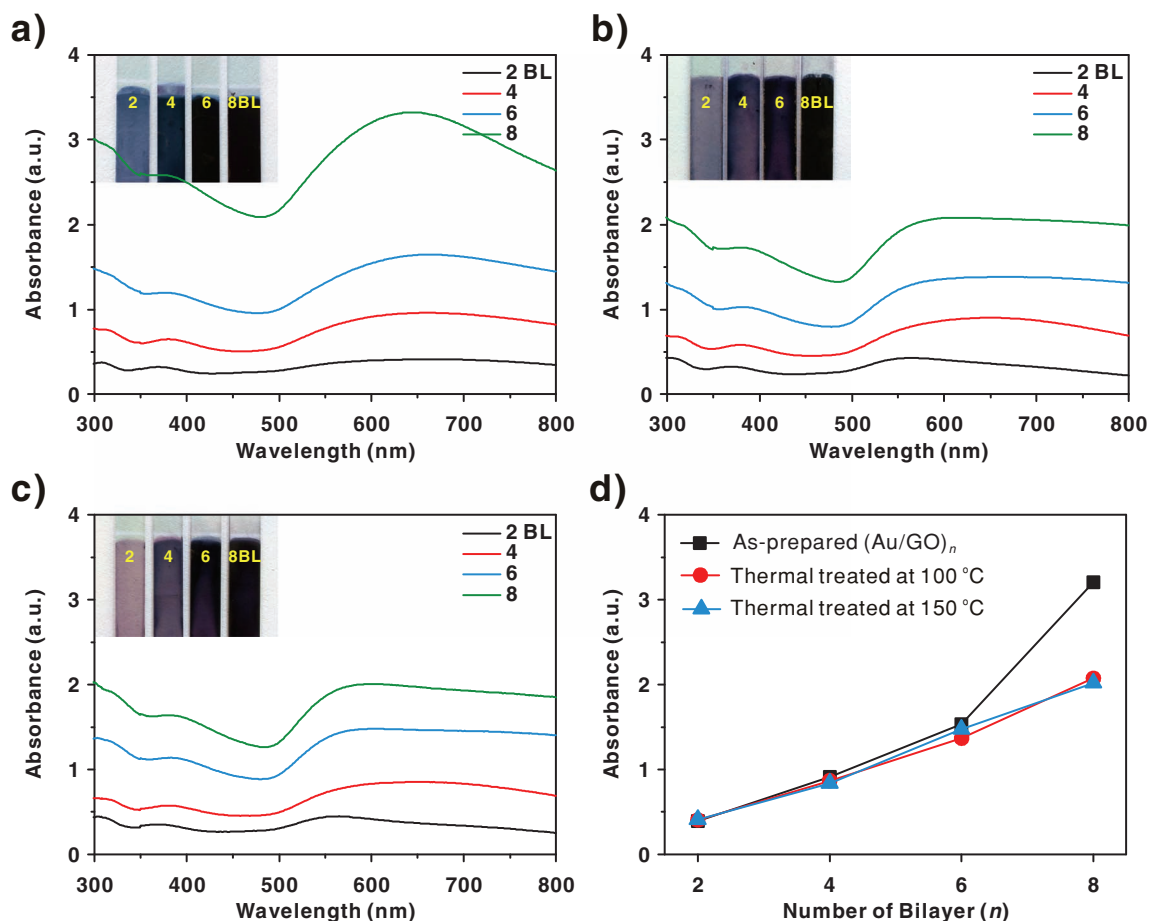


**Figure 1.** (a–c) UV/vis absorbance spectra of  $(\text{Au}/\text{GO})_n$  multilayer thin films. (a) as-prepared, (b) thermal treated at 100 °C and (c) thermal treated at 150 °C. (d) The corresponding absorbance maxima at 600 nm according to the number of bilayers. Inset image represents the samples measured.

that the surface passivating ligands play an important role in controlling the activity of NPs at the interface between NPs and electrolytes during the electrocatalytic reactions.<sup>[41]</sup> Consequently, in this study we chose two different temperatures to the melting point of DMAP ligands (110 °C), 100 °C and 150 °C to see the effect of the surface ligand mobility within the multilayers during the electrocatalytic oxidation of methanol.

As shown in Figure 1, the successful growth of multilayers was monitored by the gradual increase of characteristic surface plasmon absorbance of Au NPs within the multilayer film. As similarly observed in other report, the surface plasmon broadens when assembled within the multilayer film and exhibits the bathochromic red-shift compared to individual Au NPs ( $\lambda_{\text{max}} = 514 \text{ nm}$ ), which resulted from the coupled plasmon interactions of Au NPs in close proximity within the same layer and/or adjacent layers.<sup>[37,42]</sup> Interestingly, the absorbance of the multilayer film decreased upon thermal treatment and the overall broad spectra blue-shifted from ca. 620 nm to 540 nm, indicating the reorganization of the as-assembled Au NPs within the multilayer film. This effect is particularly pronounced in the 8-bilayer film after thermal treatment due to the increased amount of Au NPs as illustrated by the sudden drop of absorbance. In addition, the linear growth curve clearly demonstrates the uniform multilayer formation after each assembly.

According to the representative AFM images, the initial depositions of only a few layers displayed overlaid sheets of GO with a high density of Au NPs that were anchored well on the surface of the graphene nanosheets (Figure 2, see Figure S2 for more images). Interestingly, the edges of individual graphene sheets were clearly visible in the as-assembled 2-bilayer film, whereas the individual sheets appeared to stack together as the number of bilayers increased. The surface roughness generally increased with the progress of LbL assembly, regardless of the post-treatment. On the other hand, for example, surface root-mean-square roughness ( $R_{\text{rms}}$ ) values of 2- and 6-bilayers were determined to be 6.97 and 6.83 nm, respectively, which decreased to 5.65 and 6.19 nm after thermal annealing at 150 °C (averaged over  $10 \times 10 \mu\text{m}^2$ ). The decreased surface roughness can be ascribed to the reorientation of Au NPs with the increased mobility of the ligand and the densification of the thin film during thermal treatment. This observation is consistent with reduced aggregation of Au NPs within the multilayers after thermal treatment as suggested in the UV/vis spectra. Additionally, the scanning electron microscopy (SEM) and transmission electron microscopy (TEM) images illustrate the successful deposition of Au NPs on top of the GO nanosheets leading to the increased density of Au NPs and GO nanosheet without significant changes in the size of Au NPs (Figure S3 and S4).

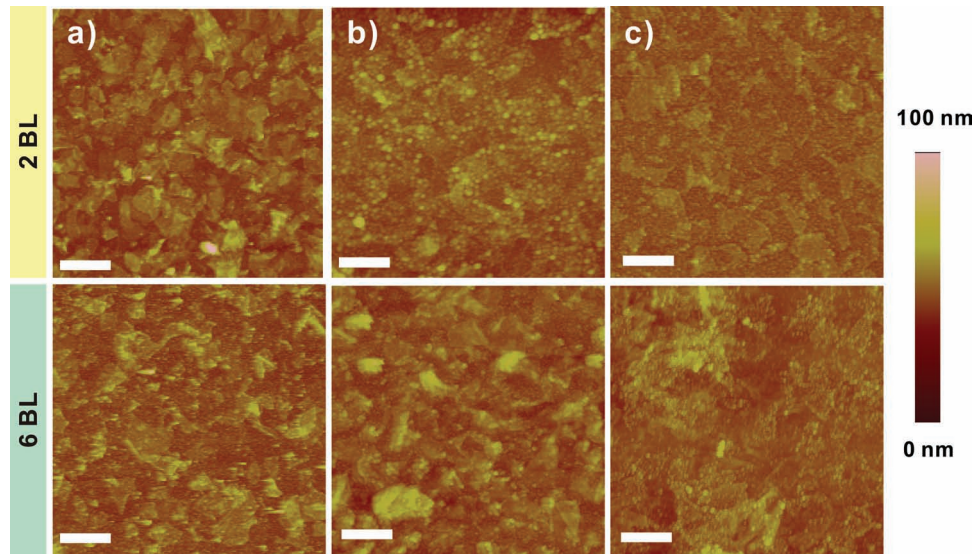
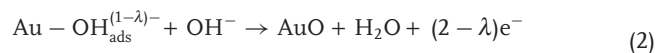
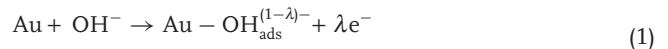


**Figure 2.** Representative AFM images of  $(\text{Au}/\text{GO})_n$  multilayer thin films of 2- and 6-bilayer. (a) as-assembled films, (b) thermal treated at 100 °C and (c) thermal treated at 150 °C. The scale bar of each image is 1  $\mu\text{m}$ . Note the surface morphology changes in the  $(\text{Au}/\text{GO})_n$  multilayer films after thermal treatment.

After careful examination of the assembled  $(\text{Au}/\text{GO})_n$  multilayers films, the electrochemical characteristics toward the oxidation of methanol were first investigated by running the cyclic voltammetry of the multilayer thin films in a 0.10 M KOH solution with and without methanol under  $\text{N}_2$  atmosphere (Figure 3). In the absence of methanol, the forward sweep shows an onset potential of 0.35 V (vs Hg/HgO), which indicates the adsorption of  $\text{OH}^-$  and subsequent formation of

surface oxide on Au NPs at a higher potential as described in the following Reactions (1) and (2).



where  $\text{OH}_{\text{ads}}^-$  represents the directly chemisorbed  $\text{OH}^-$  on Au, and the charge transfer coefficient  $\lambda$  varies between 0 and

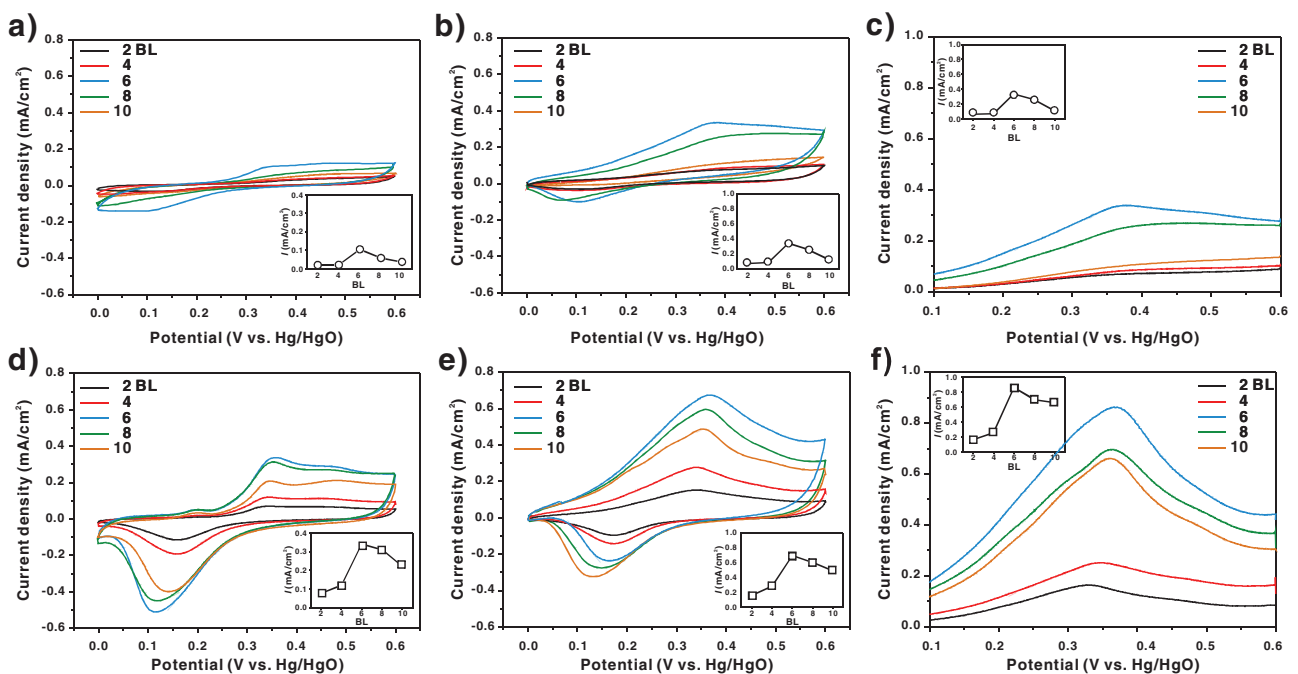


**Figure 3.** (a,b,d,e) Cyclic voltammograms (CV) of  $(\text{Au}/\text{GO})_n$  multilayer thin films thermal treated at (a) 100 °C and (d) 150 °C samples measured in 0.10 M KOH without  $\text{CH}_3\text{OH}$ . (b) 100 °C and (e) 150 °C samples measured in 0.10 M KOH with 1.0 M  $\text{CH}_3\text{OH}$ . (c, f) Linear sweep voltammetry (LSV) of  $(\text{Au}/\text{GO})_n$  thin films thermal treated at (c) 100 °C and (f) 150 °C measured in 0.10 M KOH with 1.0 M  $\text{CH}_3\text{OH}$ . The insets in all images show the current density plot as a function of number of bilayer (BL). All measurements were carried out in a saturated  $\text{N}_2$  at a scan rate of 20 mV/s.

1 depending on the extent of the faradaic reaction (0 for a non-faradaic reaction and 1 for a faradaic reaction).

In the backward sweep, a reduction peak at 0.12 V was observed, which corresponds to the reduction of the surface oxide layer and desorption of OH<sup>-</sup> from the Au NPs.<sup>[43]</sup> It is of note that both oxidation and reduction peaks in all samples appear nearly at the same position irrespective of the number of bilayers; however, the samples treated at 150 °C generally exhibited superior electrocatalytic activity to those treated at 100 °C. Interestingly, we found that the current density of the (Au/GO)<sub>n</sub> multilayer films treated at 150 °C increased as the number of bilayers increased, up to 6-bilayer; however, the current density subsequently diminished as in Figure 3d. When 1.0 M of methanol was added to the system, the cyclic voltammograms changed significantly; for example, large anodic current peaks at 0.38 and 0.36 V and cathodic current peak at 0.11 and 0.17 V were observed for the 6-bilayer film treated at 100 °C and 150 °C, respectively. Cyclic voltammetry of (Au/GO)<sub>6</sub> thin films thermal treated at 150 °C samples showed that the anodic peak currents are linearly proportional to the square root of scan rates, providing the electrocatalytic oxidation of methanol is governed by diffusion-controlled process (Figure S5).

The enhanced current at all voltage ranges is attributed to the improved kinetics of methanol oxidation promoted by the following catalytic conversion reaction, Equation (3) on the surface of the Au NPs with surface adsorbed OH<sup>-</sup> as well as the solution OH<sup>-</sup> that yields more number of electrons upon oxidation of methanol. In general, λ is regarded as 0 as presented in Scheme 1.

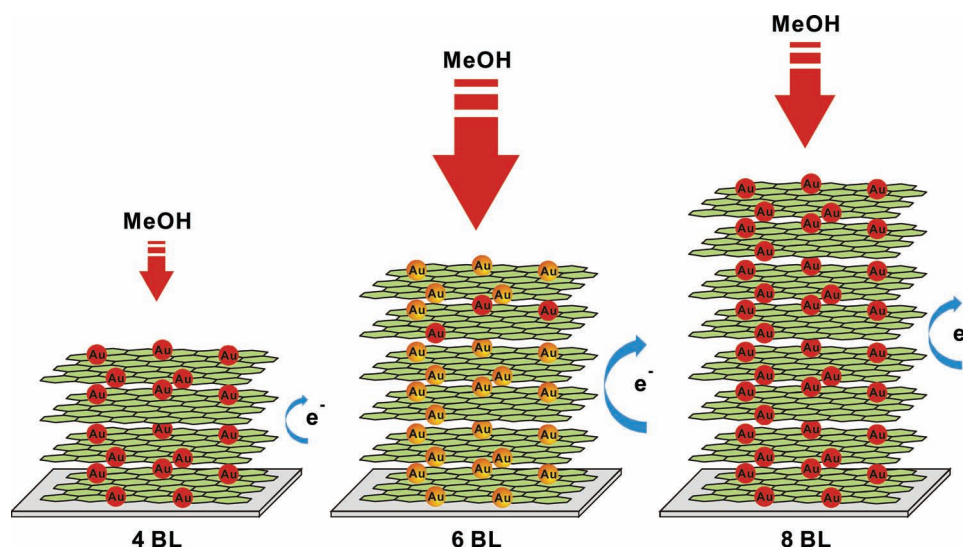


The control experiment of LbL-assembled all-GO multilayer films of (GO/GO)<sub>n</sub> did not show any measurable peak under the identical potential window, confirming the key role of Au NPs responsible for the electrocatalytic oxidation of methanol

in our system (Figure S6).<sup>[34,35,44,45]</sup> Moreover, the thermal treatment of (Au/GO)<sub>6</sub> film at a higher temperature 300 °C does not improve the electrocatalytic activity toward the methanol oxidation significantly, albeit the electronic conductivity increased considerably compared to that after thermal treatment at 150 °C, suggesting the ligand mobility atop Au NPs is critical in enhancing the overall electrocatalytic activity (Figure S6).

As demonstrated already in Figure 3d, we found that there is an optimum film thickness present when the forward anodic peak is plotted with respect to the number of bilayers (all insets in Figure 3). In all samples, the current density increased with the number of bilayers, obviously due to the increased concentration of active Au NPs within the multilayer films up to 6 bilayers. On the other hand, the forward anodic peak current began to decrease after the 6-bilayer film, possibly due to the limited diffusion of methanol into the hybrid electrode with increased thickness as well as to the reduced electron and mass transfer to outer NPs as similarly observed in other work (Scheme 2).<sup>[46]</sup> This observation features the importance of LbL assembly which can afford the precise control over the architecture of the electrode in achieving the best performance with a given set of components *via* simple electrode fabrication technique.

The active amount of Au NPs can be obtained from the inductively-coupled plasma–mass spectrometry (ICP-MS), which allows us to attain mass-specific peak currents of 44 and 90 mA/mg for the 6-bilayer film treated at 100 °C and 150 °C, respectively, in 0.10 M KOH with 1.0 M CH<sub>3</sub>OH. This value is superior to the recent report of 50 mA/mg from Pt NPs embedded within the polyelectrolyte multilayers, suggesting the highly efficient catalytic activity of a (Au/GO)<sub>n</sub> multilayer electrode without using high-cost Pt catalyst.<sup>[46]</sup> Also, Zhang and co-workers reported 48.6 mA/mg in 0.10 M KOH and 5.0 M CH<sub>3</sub>OH with Au NPs supported on a commercial activated carbon (Vulcan XC-72R).<sup>[47]</sup> In case of our (Au/GO)<sub>6</sub> film after 150 °C treatment, we found significantly higher catalytic activity of 273 mA/mg under the identical reaction condition.



**Scheme 2.** Schematic representation of the possible mechanism of electrocatalytic activity of (Au/GO)<sub>n</sub> toward methanol oxidation depending on the number of bilayers (BL). Two factors such as methanol diffusion into the electrode and electron and mass transfer from the electrode govern the fine balance of multilayered hybrid electrode in the observed electrocatalytic activity.

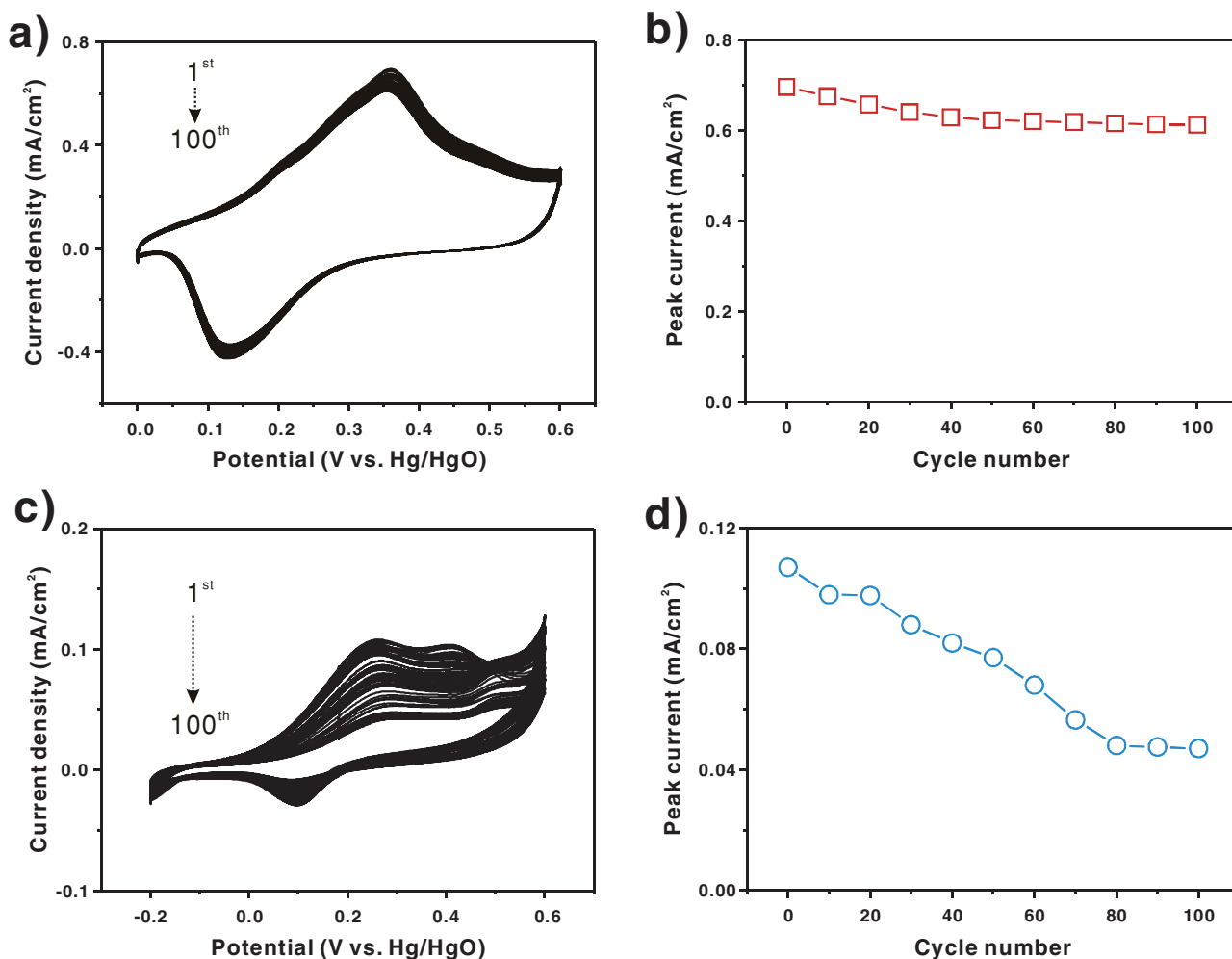


**Figure 4.** Cyclic voltammetry stability test of (a, b)  $(\text{Au}/\text{GO})_6$  thin film thermal treated at  $150\text{ }^\circ\text{C}$  samples, (c, d) DMAP-Au NPs on a glassy carbon electrode. Both samples were measured in  $0.10\text{ M KOH}$  with  $1.0\text{ M CH}_3\text{OH}$  in a saturated  $\text{N}_2$  at a scan rate of  $20\text{ mV/s}$ . Identical concentration of Au NPs was used for comparison.

Although more stringent stability tests are necessary in order to meet the requirements for actual fuel cell performance, we observe that the multiple electrocatalytic cycles of  $(\text{Au}/\text{GO})_6$  films thermal treated at  $150\text{ }^\circ\text{C}$  show a stable electrochemical response over 100 cycles with a retention of 88% (Figure 4a and b). In a clear contrast, the free Au NPs without GO support have a significantly lower cyclic stability of 44% with a low current density ( $0.107\text{ mA/cm}^2$  vs  $0.696\text{ mA/cm}^2$  of  $(\text{Au}/\text{GO})_6$  film), emphasizing the critical role of graphene nanosheet as a chemically stable support in preserving the catalytic active surface of Au NPs during electrochemical cycles (Figure 4c and d). Moreover, the Au NPs supported on conductive amorphous Ketjen Black does not show comparable stability (52.3%), suggesting a unique 3-dimensional LbL structure is critical in preventing the coalescence of high surface energy Au NPs each other (Figure S7).

Further investigation was made into the electrochemical characteristics of methanol oxidation in the 6-bilayer  $(\text{Au}/\text{GO})_6$  film after thermal treatment at  $150\text{ }^\circ\text{C}$ . Under the increasing

concentration of methanol, the anodic peak current ( $i_a$ ) increased linearly with methanol concentration as shown in Figure 5.

The cathodic peak current ( $i_c$ ), on the other hand, decreased with increasing methanol concentration, which could be attributed to reduced Au oxide coverage upon sweeping to negative potential. Figure 5b displays the Tafel plot of the methanol oxidation as a function of methanol concentration at a scan rate of  $20\text{ mV/s}$ . The Tafel plot has two distinct linear ranges that change its slope significantly at  $0.15\text{ V}$ , corresponding to the potential of maximum cathodic peak current. The Tafel slope of  $267 \pm 2.4\text{ mV/dec}$  is obtained for the potential range of  $0.15\text{--}0.25\text{ V}$  with a calculated transfer coefficient,  $\alpha n$ , of  $0.22$ . This suggests that the first charge transfer is the rate-determining step.<sup>[48–50]</sup> The overall reaction order of methanol oxidation with respect to the concentration of methanol can be estimated from the slope of linear fit of  $0.89$  at different potentials (Figure S8), which suggests that the methanol oxidation mechanism in the Tafel ranges remains constant irrespective of increasing concentration of methanol.<sup>[47]</sup>

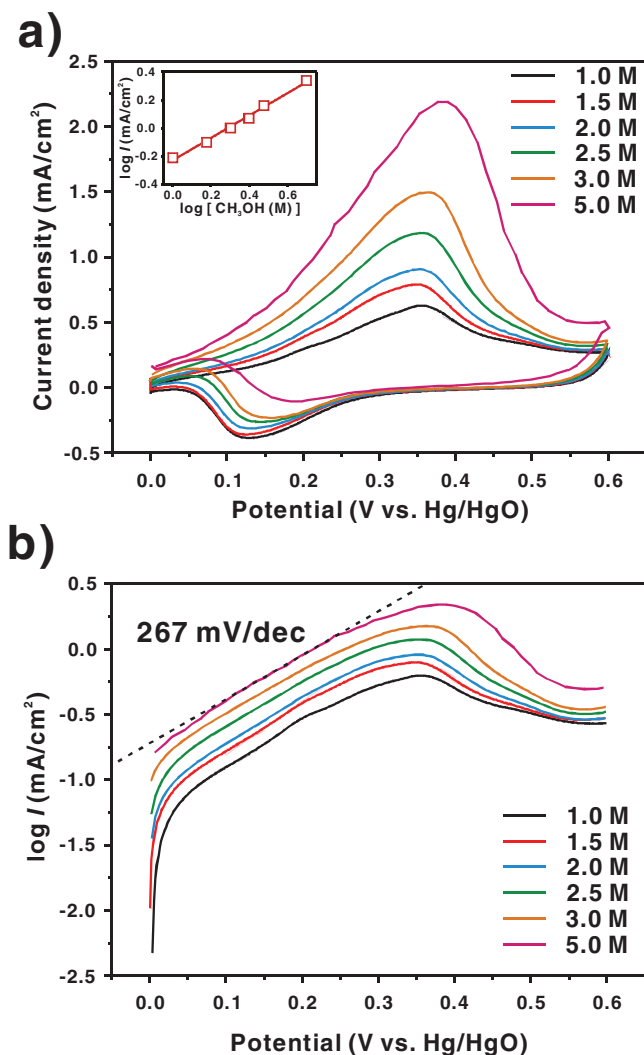


**Figure 5.** (a) Cyclic voltammograms of  $(\text{Au}/\text{GO})_6$  thin film thermal treated at  $150\text{ }^\circ\text{C}$  in  $0.10\text{ M}$  KOH with different concentrations of  $\text{CH}_3\text{OH}$ . Inset shows the plot of  $\log(i)$  against  $\log(\text{CH}_3\text{OH})$  at different concentrations of  $\text{CH}_3\text{OH}$ . (b) The corresponding Tafel plot with a representative linear fit. All measurements were carried out in a saturated  $\text{N}_2$  at a scan rate of  $20\text{ mV/s}$ .

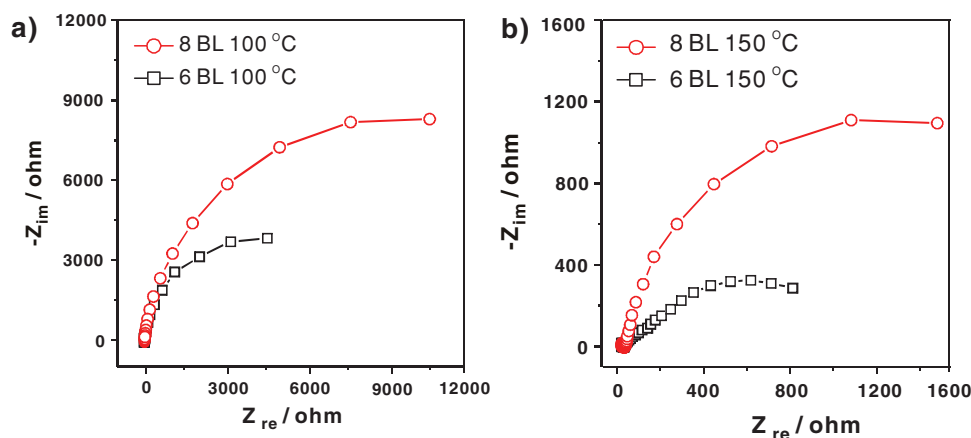


**Figure 6.** Nyquist plots of impedance on  $(\text{Au}/\text{GO})_n$  thin films in  $0.10\text{ M}$  KOH and  $1.0\text{ M}$   $\text{CH}_3\text{OH}$  solution measured at  $0.35\text{ V}$ . (a) 6- and 8-bilayer films after thermal treatment at  $100\text{ }^\circ\text{C}$ , and (b) at  $150\text{ }^\circ\text{C}$ .

Electrochemical impedance spectroscopy provides good information of the kinetics and interfacial resistance that are critical in the evaluation of the electrochemical reactions.<sup>[51,52]</sup> The charge transfer resistances ( $R_{ct}$ ) of the methanol oxidation reaction at the surface of Au NPs within the  $(\text{Au}/\text{GO})_n$  multilayer film are measured with varying number of bilayers and thermal treatment. As demonstrated in **Figure 6**, the Nyquist plot determined the  $R_{ct}$  values of 6-bilayer films that are for lower than those of 8-bilayer film, such as  $7362\text{ ohm}$  (6 bilayer) and  $18807\text{ ohm}$  (8 bilayer) in  $100\text{ }^\circ\text{C}$  treated samples and  $118.3\text{ ohm}$  (6 bilayer) and  $1859\text{ ohm}$  (8 bilayer) in  $150\text{ }^\circ\text{C}$  samples, respectively. This result indicates the 6-bilayer films possess the better electrocatalytic performance than that of the 8-bilayer film which is in good agreement with the previous data.<sup>[53]</sup> The Nyquist plot also clearly supports the claim that heat treatment at  $150\text{ }^\circ\text{C}$  can reduce the interfacial resistance of Au NPs for an enhanced catalytic activity toward methanol oxidation. Once again, this supports our postulation of the enhanced mobility of surface ligand upon heat treatment above its melting point.

In addition, when we increased the assembly pH of GO from 4 to 11, the electrocatalytic activity could be further controlled due to the changes in the amount of Au NPs on the graphene sheets as well as the internal structure of electrode, which led to influence the overall catalytic activity (Figure S9). This result further highlights the potential of LbL assembly in fine tuning the catalytic activity of the current system toward the development of more efficient electrocatalyst and it will be the subject of our on-going endeavour.

### 3. Conclusion

In conclusion, we have developed a simple approach for integrating electroactive gold nanoparticles (Au NPs) with graphene oxide (GO) nanosheet support by layer-by-layer (LbL) assembly for the creation of 3-dimensional electrocatalytic thin films that are active toward methanol oxidation. This approach involves the electrostatic interaction of two oppositely charged suspensions of the GO nanosheet with Au NPs. The LbL method can not only control the amount of Au NPs on a graphene sheet,

but also enhance the stability of Au NPs when combined with graphene sheet. Furthermore, the Au-GO hybrid multilayer was successfully employed in the catalytic activity of methanol oxidation in alkaline conditions. Through careful investigations of the catalyst, we could control the catalytic efficiency with changes of the number of bilayers and thermal treatment temperature. Because of the highly versatile and tunable properties of LbL-assembled thin films of hybrid electrocatalyst, we anticipate that the general concept presented here offers a new design of electrocatalyst for direct methanol fuel cell (DMFC). Considering the wide-ranging potential applications of a two-dimensional graphene sheet as a host material for a variety of NPs, the approach developed here may lead to new possibilities for the fabrication of hybrid NP-graphene structures endowed with multiple functionalities.

#### 4. Experimental Section

**Preparation of DMAP-Au nanoparticles:** The DMAP-Au nanoparticles were prepared according to a literature method.<sup>[38]</sup> In brief, 30 mM aqueous metal chloride solution ( $\text{HAuCl}_4 \cdot 3\text{H}_2\text{O}$ , 30 mL) was added to a 25 mM solution of tetraoctylammonium bromide in toluene (80 mL). A 0.40 M solution of freshly prepared  $\text{NaBH}_4$  (25 mL) was added to the stirred mixture, which caused an immediate reduction to occur. After 30 min, the two phases were separated and the toluene phase was subsequently washed with 0.10 M  $\text{H}_2\text{SO}_4$ , 0.10 M  $\text{NaOH}$ , and  $\text{H}_2\text{O}$  (three times), and then dried over anhydrous  $\text{Na}_2\text{SO}_4$ . An aqueous 4-dimethylaminopyridine (DMAP) solution (0.10 M, 1.0 mL) was added to aliquots (1.0 mL) of the as-prepared nanoparticle mixtures. This concentration of DMAP was found to be sufficient to affect the complete and spontaneous phase transfer of the nanoparticles. Direct phase transfer across the organic/aqueous boundary was completed within 1 h without additional stirring.

**Preparation of GO:** Graphite oxide was synthesized from graphite powder (Aldrich) by modified Hummers method and exfoliated to give a brown dispersion of graphene oxide (GO) under ultrasonication.<sup>[36]</sup>

**Layer-by-layer assembly of  $(\text{Au}/\text{GO})_n$  multilayer film:** Silicon and ITO-coated glass substrate was cleaned by piranha solution to remove any organic contamination and treated with (3-aminopropyl) triethoxysilane to introduce hydrophilic and positively charged surface. The substrate was dipped into negatively charged GO solution (0.5 mg/mL) at pH 4 for 10 min. It was then dipped into DI water for 1 min three times to remove loosely bound GO. Subsequently, the substrate was then dipped into positively charged DMAP-coated Au NPs solution for 10 min, and washed with DI water three times for 1 min, which afford one-bilayer film of  $(\text{Au}/\text{GO})_1$ . The above procedures were repeated to achieve the desired number of bilayers. These as-assembled  $(\text{Au}/\text{GO})_n$  multilayer films were subjected thermal reduction at 100 °C or 150 °C for 12 h in an oven.

**Electrocatalytic characterizations:** Electrochemical experiments were performed on Biologic science instrument, VSP using a standard three electrode cell. A platinum wire was used as a counter electrode and  $\text{Hg}/\text{HgO}$  as a reference. The working electrode was  $(\text{Au}/\text{GO})_n$  multilayer thin film. Cyclic voltammetry (CV) and linear sweep voltammetry (LSV) were performed between 0.0 to 0.6 V in 0.1 M KOH solution with or without 1.0 M methanol solution at room temperature at a scan rate of 20 mV/s. Electrochemical impedance spectroscopy (EIS) measurements were carried out in the frequency range from 100 kHz to 100 mHz under AC stimulus of 10 mV in amplitude.

**Other characterizations:** The  $\zeta$ -potential of colloidal suspensions was measured using a zeta potential analyzer (Malvern, Zetasizer nano-zs). The absorbance of the thin films was characterized by using UV/vis spectroscopy (VARIAN, Cary 5000). The surface morphology of the samples was investigated using atomic force microscopy (AFM,

Nanoscope V, Veeco) via a tapping mode, scanning electron microscopy (SEM, FEI, NOVA NANOSEM230) and transmission electron microscope (TEM, Carl Zeiss-LIBRA 120).

#### Supporting Information

Supporting Information is available from the Wiley Online Library or from the author.

#### Acknowledgements

This research was supported by WCU (World Class University) program through the Korea Science and Engineering Foundation funded by the Ministry of Education, Science and Technology (R31-2008-000-20012-0), by the National Research Foundation of Korea (NRF) funded by the Ministry of Education, Science and Technology (MEST) (2010-0003219) and also supported by the New & Renewable Energy of the Korea Institute of Energy Technology Evaluation and Planning (KETEP) grant funded by the Korea government Ministry of Knowledge Economy (20113020030060).

Received: March 27, 2012

Revised: April 23, 2012

Published online: July 26, 2012

- [1] T. Yamaguchi, H. Zhou, S. Nakazawa, N. Hara, *Adv. Mater.* **2007**, *19*, 592.
- [2] Z. H. Wen, J. Liu, J. H. Li, *Adv. Mater.* **2008**, *20*, 743.
- [3] C. J. Zhong, J. Luo, B. Fang, B. N. Wanjala, P. N. Njoki, R. Loukrakpam, J. Yin, *Nanotechnology* **2010**, *21*, 062001.
- [4] A. S. Arico, P. Bruce, B. Scrosati, J. M. Tarascon, W. van Schalkwijk, *Nat. Mater.* **2005**, *4*, 366.
- [5] Y. S. Hu, Y. G. Guo, W. Sigle, S. Hore, P. Balaya, J. Maier, *Nat. Mater.* **2006**, *5*, 713.
- [6] M. R. Gao, Q. Gao, J. Jiang, C. H. Cui, W. T. Yao, S. H. Yu, *Angew. Chem. Int. Ed.* **2011**, *50*, 4905.
- [7] J. Kua, W. A. Goddard, *J. Am. Chem. Soc.* **1999**, *121*, 10928.
- [8] L. D. Burke, J. A. Collins, M. A. Horgan, L. M. Hurley, A. P. O'Mullane, *Electrochim. Acta* **2000**, *45*, 4127.
- [9] Y. Song, R. M. Garcia, R. M. Dorin, H. R. Wang, Y. Qiu, E. N. Coker, W. A. Steen, J. E. Miller, J. A. Shelnett, *Nano Lett.* **2007**, *7*, 3650.
- [10] Y. Sun, L. Zhuang, J. Lu, X. Hong, P. Liu, *J. Am. Chem. Soc.* **2007**, *129*, 15465.
- [11] M. M. Maye, Y. B. Lou, C. J. Zhong, *Langmuir* **2000**, *16*, 7520.
- [12] Y. B. Lou, M. M. Maye, L. Han, J. Luo, C. J. Zhong, *Chem. Commun.* **2001**, 473.
- [13] A. Haruta, *Chem. Rec.* **2003**, *3*, 75.
- [14] J. A. Rodriguez, P. Liu, J. Hrbek, J. Evans, M. Perez, *Angew. Chem. Int. Ed.* **2007**, *46*, 1329.
- [15] E. Yoo, T. Okata, T. Akita, M. Kohyama, J. Nakamura, I. Honma, *Nano Lett.* **2009**, *9*, 2255.
- [16] Y. J. Gao, D. Ma, G. Hu, P. Zhai, X. H. Bao, B. Zhu, B. S. Zhang, D. S. Su, *Angew. Chem. Int. Ed.* **2011**, *50*, 10236.
- [17] Y. Y. Liang, Y. G. Li, H. L. Wang, J. G. Zhou, J. Wang, T. Regier, H. J. Dai, *Nat. Mater.* **2011**, *10*, 780.
- [18] S. Stankovich, D. A. Dikin, G. H. B. Dommett, K. M. Kohlhaas, E. J. Zimney, E. A. Stach, R. D. Piner, S. T. Nguyen, R. S. Ruoff, *Nature* **2006**, *442*, 282.
- [19] A. A. Balandin, S. Ghosh, W. Z. Bao, I. Calizo, D. Teweldebrhan, F. Miao, C. N. Lau, *Nano Lett.* **2008**, *8*, 902.

- [20] Z. Lee, K. J. Jeon, A. Dato, R. Erni, T. J. Richardson, M. Frenklach, V. Radmilovic, *Nano Lett.* **2009**, 9, 3365.
- [21] K. S. Novoselov, D. Jiang, F. Schedin, T. J. Booth, V. V. Khotkevich, S. V. Morozov, A. K. Geim, *P. Natl. Acad. Sci. USA* **2005**, 102, 10451.
- [22] G. Eda, G. Fanchini, M. Chhowalla, *Nat. Nanotechnol.* **2008**, 3, 270.
- [23] K. S. Kim, Y. Zhao, H. Jang, S. Y. Lee, J. M. Kim, K. S. Kim, J. H. Ahn, P. Kim, J. Y. Choi, B. H. Hong, *Nature* **2009**, 457, 706.
- [24] Y. G. Zhou, J. J. Chen, F. B. Wang, Z. H. Sheng, X. H. Xia, *Chem. Commun.* **2010**, 46, 5951.
- [25] Z. S. Wu, D. W. Wang, W. Ren, J. Zhao, G. Zhou, F. Li, H. M. Cheng, *Adv. Funct. Mater.* **2010**, 20, 3595.
- [26] S. J. Guo, S. J. Dong, E. W. Wang, *ACS Nano* **2010**, 4, 547.
- [27] H. Bai, C. Li, G. Q. Shi, *Adv. Mater.* **2011**, 23, 1089.
- [28] R. Kou, Y. Shao, D. Mei, Z. Nie, D. Wang, C. Wang, V. V. Viswanathan, S. Park, I. A. Aksay, Y. Lin, Y. Wang, J. Liu, *J. Am. Chem. Soc.* **2011**, 133, 2541.
- [29] Q. T. Qu, S. B. Yang, X. L. Feng, *Adv. Mater.* **2011**, 23, 5574.
- [30] C. Z. Zhu, S. J. Guo, Y. M. Zhai, S. J. Dong, *Langmuir* **2010**, 26, 7614.
- [31] G. Decher, *Science* **1997**, 277, 1232.
- [32] P. T. Hammond, *Adv. Mater.* **2004**, 16, 1271.
- [33] T. K. Hong, D. W. Lee, H. J. Choi, H. S. Shin, B. S. Kim, *ACS Nano* **2010**, 4, 3861.
- [34] J. Hong, J. Y. Han, H. Yoon, P. Joo, T. Lee, E. Seo, K. Char, B. S. Kim, *Nanoscale* **2011**, 3, 4515.
- [35] D. W. Lee, T. K. Hong, D. Kang, J. Lee, M. Heo, J. Y. Kim, B. S. Kim, H. S. Shin, *J. Mater. Chem.* **2011**, 21, 3438.
- [36] W. S. Hummers, R. E. Offeman, *J. Am. Chem. Soc.* **1958**, 80, 1339.
- [37] D. Li, M. B. Muller, S. Gilje, R. B. Kaner, G. G. Wallace, *Nat. Nanotechnol.* **2008**, 3, 101.
- [38] D. I. Gittins, F. Caruso, *Angew. Chem. Int. Ed.* **2001**, 40, 3001.
- [39] W. F. Chen, L. F. Yan, *Nanoscale* **2010**, 2, 559.
- [40] J. Kwon, S. H. Lee, K. H. Park, D. H. Seo, J. Lee, B. S. Kong, K. Kang, S. Jeon, *Small* **2011**, 7, 864.
- [41] L. J. Burcham, M. Badlani, I. E. Wachs, *J. Catal.* **2001**, 203, 104.
- [42] W. Y. Yuan, C. M. Li, *Langmuir* **2009**, 25, 7578.
- [43] K. A. Assiombon, D. Roy, *Surf. Sci.* **2005**, 594, 99.
- [44] J. Hong, K. Char, B. S. Kim, *J. Phys. Chem. Lett.* **2010**, 1, 3442.
- [45] H. Hwang, P. Joo, M. S. Kang, G. Ahn, J. T. Han, B. S. Kim, J. H. Cho, *ACS Nano* **2012**, 6, 2432.
- [46] X. Zhang, X. J. Zan, Z. H. Su, *J. Mater. Chem.* **2011**, 21, 17783.
- [47] S. H. Yan, S. C. Zhang, Y. Lin, G. R. Liu, *J. Phys. Chem. C* **2011**, 115, 6986.
- [48] J. Luo, P. N. Njoki, Y. Lin, D. Mott, L. Y. Wang, C. J. Zhong, *Langmuir* **2006**, 22, 2892.
- [49] A. Kowal, M. Li, M. Shao, K. Sasaki, M. B. Vukmirovic, J. Zhang, N. S. Marinkovic, P. Liu, A. I. Frenkel, R. R. Adzic, *Nat. Mater.* **2009**, 8, 325.
- [50] W. E. Mustain, J. Prakash, *J. Power Sources* **2007**, 170, 28.
- [51] E. P. Lee, Z. M. Peng, W. Chen, S. W. Chen, H. Yang, Y. N. Xia, *ACS Nano* **2008**, 2, 2167.
- [52] B. Y. Chang, S. M. Park, *Annu. Rev. Anl. Chem.* **2010**, 3, 207.
- [53] J. Kim, S. W. Lee, P. T. Hammond, Y. Shao-Horn, *Chem. Mater.* **2009**, 21, 2993.